EUROPEAN ORGANIZATION FOR NUCLEAR RESEARCH

CERN – PS DIVISION

CERN/PS 99-060 (DI)

THE RF CYCLE OF THE PIMMS SYNCHROTRON

M. Crescenti[1)], *P. Knaus*[2)] *and S. Rossi*[1)]

Abstract

This paper deals with the study of the rf cycle of the synchrotron of the Proton-Ion Medical Machine Study (PIMMS) hosted at CERN. The cycle comprises the adiabatic trapping, the acceleration and the rf gymnastics, both for protons and fully stripped carbon ions. The injection energy is 20 MeV for protons and 7 MeV/u for carbon. The maximum extraction energies are 250 MeV for protons and 400 MeV/u for carbon ions. The reserved time is less than 1 s, with a maximum magnetic field ramp of less than 3 T/s. The simulations show that the beam stays inside the aperture of the machine, and that there are no longitudinal losses. At the end of the cycle the beam is ready for extraction with a $\Delta p/p$ of 0.4 %. The peak rf voltage is 3 kV and the frequency range is from 0.49 to 2.85 MHz.

Geneva, Switzerland
November 2, 1999

[1)] TERA Foundation and Unpaid Associates of the CERN EP Division.
[2)] CERN/SL and TERA Foundation.

1. INTRODUCTION

At the beginning of 1996, a four-way collaboration between CERN, GSI, Med-AUSTRON and TERA, denominated PIMMS (*Proton-Ion Medical Machine Study*), was launched to design an optimised synchrotron for hadrontherapy. This paper deals with the study of the rf cycle of the machine both for protons and carbon ions. The description of the cycle for particle acceleration is given. Then the different phases of the rf cycle are analysed and discussed in detail: the capture process, the acceleration and the beam gymnastics to prepare the beam for resonant extraction. The study has been performed using analytical and tracking codes and takes into account space-charge effects that are particularly relevant for protons at injection and in the early phases of acceleration. The injection energy is 20 MeV for protons and 7 MeV/u for carbon ions. Extraction energies range from 60 to 250 MeV for protons and from 120 to 400 MeV/u for carbon ions. The cycles for 250 MeV protons and for 400 MeV/u carbon ions are presented. In Appendix A, a brief reminder is given of the basic expressions used in the analyses. In Appendix B the cycles for 60 MeV protons and for 120 MeV/u carbon ions are presented. A brief introduction to the space-charge code is given in Appendix C.

The three tools used for the computations are the following:

- RFAC, *Radio Frequency Analytical Code* developed for this purpose.
- ESME [1], a multi-particle tracking code, well known in the accelerators community, available for protons.
- TSC1D [2], *Tracking with Space Charge 1D*, a multi-particle tracking code recently developed. It takes into account the longitudinal space charge contribution.

For a perfect adiabatic cycle, RFAC describes precisely the evolution of the beam parameters during the cycle. Beam emittance dilution due to the longitudinal space-charge force is not taken into account. In reality, the cycle cannot be perfectly adiabatic and the contribution of the space-charge force cannot be neglected. The imperfect adiabaticity is taken into account in ESME and in TSC1D simulations. TSC1D in addition considers the longitudinal space-charge contribution.

The rms bunch length and rms energy spread values of the accelerated bunch, calculated with the three codes, are compared in Figure 1. Only the last few milliseconds of the adiabatic trapping are considered and the first few milliseconds of acceleration, that is the most critical part. The values from TSC1D are about 10% higher due to the space-charge effect.

The transverse beam dimensions have been evaluated using a uniformly filled ellipsoid in 3-D (1-D parabolic distribution). The longitudinal beam distribution of the debunched beam is also considered to be parabolic in momentum.

According to [3], the beam model used in the analytical evaluation of the space-charge effect leads to a consideration of a parabolic beam distribution in 2-D transverse space.

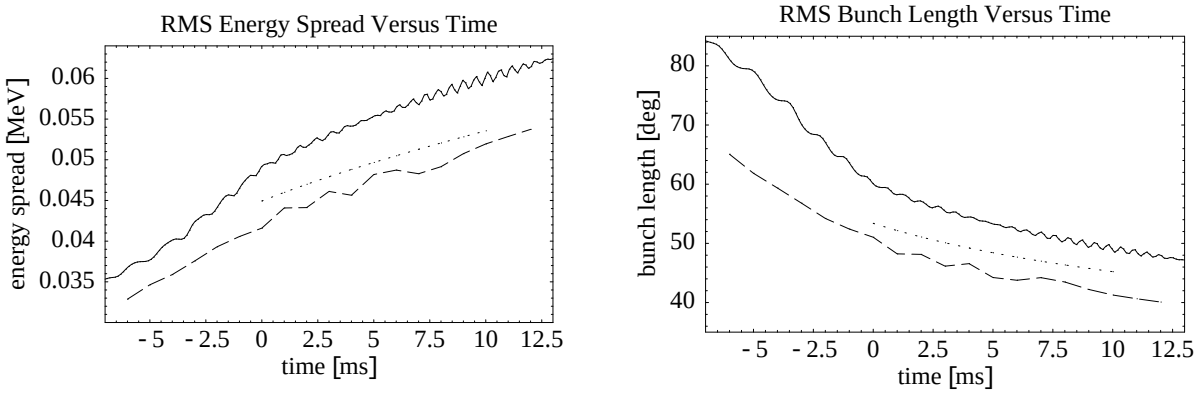

Fig. 1. *20-250 MeV protons. Comparison of the rms bunch energy spread (left) and of the rms bunch length (right) at the most critical times. Continuous line: TSC1D, dotted line: RFAC, hashed line: ESME. Due to space charge, TSC1D values are about 15 - 20 % larger.*

The procedure of optimisation of the cycle is as follows. One starts with RFAC code for the proton cycle. The results are then checked with the code ESME. The adiabatic factor (for definition see paragraph 4) is kept quite small, so that the results are very similar. RFAC is then used to compute the cycle of the ions trying to keep the same or smaller adiabatic factor. The input parameters are varied in order to keep the beam transverse dimensions within the acceptance of the machine. A safety margin is chosen to avoid both transverse and longitudinal losses. Then both cycles, protons and ions, are used as input for TSC1D code. The results of TSC1D are different due to the space-charge contribution, and overtake the safety margin. RFAC input parameters are therefore changed to increase the safety margin, and the output is again used as input for TSC1D. After a few iterations the cycles are optimised for zero losses.

2. INTRODUCTION TO TSC1D

RFAC is a computing program making use of the set of equations reported in Appendix A. ESME is a code well-known to the accelerator community. An introduction to TSC1D, the space-charge code used in the present analysis, is given in Appendix C, but for a complete understanding of the method one has to refer to [2].

The equations to treat the synchrotron motion are [4], [5]:

$$\frac{d}{dt}\left(\frac{\Delta \mathrm{E}}{h\omega_s}\right) = \frac{q}{2\pi h}\left[V(\phi) - V(\phi_s) + V_{SC}(\phi)\right] \qquad (1)$$

$$\frac{d}{dt}\Delta\phi = -\frac{h\omega_s \eta}{\beta^2 E}\Delta E \qquad (2)$$

where $\Delta E = E - E_s$, $\Delta\phi = \phi - \phi_s$, $\eta = 1/\gamma^2 - 1/\gamma_t^2$ with γ_t being the Lorentz γ at transition. E and ϕ are the total energy and the phase of the particle, $V(\phi)$ is the instantaneous applied rf voltage and h the harmonic number. The suffix "s" refers to the

synchronous particle and, since the equations govern only first-order variations from the synchronous values, the revolution frequency ω_s is evaluated for the synchronous particle. The space-charge voltage V_{SC} generated within the beam is given by the derivative of the line density $\lambda(\phi)$ of the particle distribution

$$V_{SC}(\phi) = -q\frac{d\lambda(\phi)}{d\phi}\cdot\frac{hg_0}{2\varepsilon_0\gamma^2}, \qquad (3)$$

where ε_0 is the permittivity of free space. This voltage decreases the effective rf voltage, causing an increase of bunch length. It also results in a distortion of the bunch shape, because $\frac{d\lambda}{d\phi}$ changes along the bunch. For long bunches of a beam with circular cross-section of mean radius *a* in a circular pipe of radius *b*, the geometry factor g_0 is defined as:

$$g_0 = 1 + 2\ln(b/a) \qquad (4)$$

The inductance of the vacuum chamber wall can be neglected in the present problem, because the beam energy is low.

3. THE TIMING

The basic rf cycle is composed of four parts:

- adiabatic trapping at fixed frequency (flat bottom);
- acceleration with rf frequency increase;
- rf gymnastics at fixed frequency (flat top);
- rf frequency decrease to the starting point (no beam).

The following paper will concentrate on the first three points. The adiabatic trapping needs a maximum of 40.4 ms, whilst for the preparation of the beam for extraction a maximum of 30 ms is reserved. In order to avoid beam losses the rf cycle has to follow the synchrotron magnetic cycle, which was chosen initially [6]. From this choice a maximum acceleration time of 694 ms is considered for the acceleration part to reach the maximum extraction energy, i.e. the carbon beam extracted at 400 MeV/u. For lower extraction energies, this time is scaled with the beam magnetic rigidity, see Table 1.

Table 1. *Timing for the considered cycles.*

Type of Particle	Energy [MeV/u]	Trapping [ms]	Acceleration [ms]	Preparation for extraction [ms]	Total [ms]
p^+	20-60	26.8	110.8	30	167.6
p^+	20-250	26.8	259.0	30	315.8
$^{12}C^{6+}$	7-120	40.4	340.0	22	402.4
$^{12}C^{6+}$	7-400	40.4	694.0	22	756.4

4. THE CAPTURE PROCESS

The injection scheme injects 6.84×10^{10} protons and 7.90×10^{8} carbon ions. Before capture, the beam circulating in the machine is unbunched, i.e. phase spread $\Delta\phi = 360°$, and occupies a rectangle in the longitudinal phase space. The distribution is considered uniform in phase and parabolic in energy [3]. To capture the injected particles into an rf bucket, harmonic number $h = 1$, the adiabatic trapping process is adopted [7]. The rf cavity creates a stationary bucket (phase during capture equals to 0°) with a longitudinal phase-space area small with respect to the unbunched beam dimensions. The rf voltage is then progressively increased until the bucket acceptance is large enough to accommodate the beam. At the end of the process the beam is bunched, i.e. $\Delta\phi < 360°$. The final ratio between the bunch and the bucket areas is called the filling factor.

The capture process is called adiabatic if its duration is long compared to the synchrotron period (T_s) which is considered as the typical time unit of the longitudinal dynamics. In our case, T_s is of the order of 1 ms. In this case the bunch is matched to the bucket and follows the bucket variations.

The bunch parameters at the end of the process are determined by the final bucket parameters and by the initial beam emittance (i.e. bunch length and momentum spread). A monitor of the adiabaticity of the process is given by the so-called adiabatic factor α that can be defined as:

$$\alpha = \left| \frac{\frac{dA_B}{dt} T_s}{A_B} \right| \qquad (5)$$

where A_B is the bucket area. When α increases, the variation of the bucket area in the unit time increases and the adiabaticity of the process decreases. Acceptable values are $\alpha < 0.5$ [8]. The value chosen for the definition of the capture process is $\alpha = 0.1$.
The law that describes the rf voltage increase during the capture process is given by:

$$V(t) = \frac{V_{final}}{\left[\left(\frac{V_{final}}{V_{initial}} \right)^{\frac{1}{2}} - \frac{\alpha}{T_s} t \right]^2} \qquad (6)$$

where $V_{initial}$ and V_{final} are the rf voltage values at the beginning and at the end of the trapping, respectively. The variation of the rf voltage versus time is plotted in Figure 2.

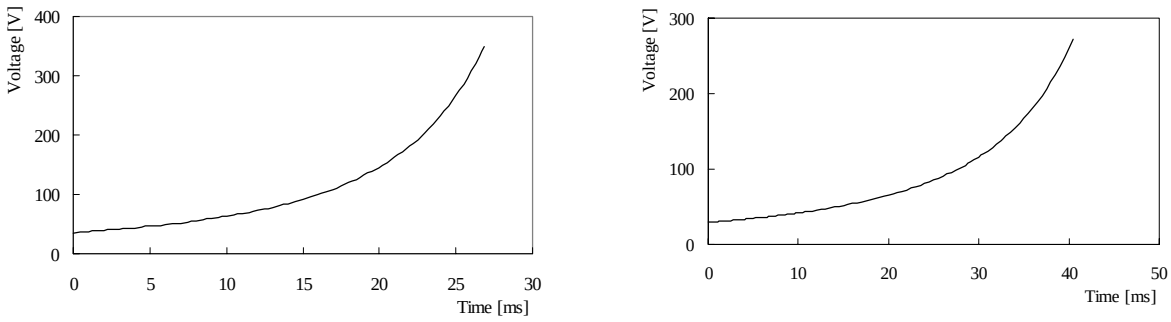

Fig. 2. *Iso-adiabatic voltage law for trapping: left) protons 20 MeV, right) carbon ions 7 MeV/u.*

The bucket area is proportional to the square root of the voltage. At the end of the process the bucket A_B and the bunch A_b areas are proportional ($K_{area} = A_B/A_b$). The choice of K_{area} fixes this ratio, which, in case of a perfectly adiabatic process, is the inverse of the filling factor. In reality, the cycle cannot be perfectly adiabatic and the actual area of the bunch increases slightly. A safety margin is maintained choosing $K_{area} \sim 1.5$.

The choice of K_{area} is used to calculate the required A_B , in the hypothesis that A_b does not increase, and then the final voltage of the adiabatic trapping. The ratio between final and initial voltage defines the bucket at the beginning of the capture process. It has been chosen $V_{final} / V_{initial} = 10$. This ratio, together with V_{final}, α and T_s, determines the trapping duration.

The previous choices define the trapping process completely and they have been chosen to satisfy the following criteria:

- the capture efficiency (i.e. the ratio between the injected and captured particles) has to be as close as possible to one;
- the dilution (i.e. the increase of the longitudinal emittance during the capture) has to be as small as possible;
- the bunching factor (i.e. the ratio between the longitudinal length of the bunch and the rf wavelength) has to be as large as possible, to reduce space-charge forces.

The adiabatic trapping process eventually produces an increase of the bunch momentum spread given by [7]:

$$\left(\frac{\Delta p}{p}\right)_{b,captured} \geq \frac{\pi}{2}\left(\frac{\Delta p}{p}\right)_{b,initial} \qquad (7)$$

The momentum spread of the captured beam depends also from the choice of $K_{area.}$ Summarised in Table 2 are the relevant parameters for the trapping process.

Table 2. *Adiabatic trapping, relevant parameters.*

	Protons	$^{12}C^{6+}$
Number of injected particles	6.84×10^{10}	7.9×10^{8}
Trapping efficiency (from simulations) [%]	100	
Kinetic energy at injection [MeV] and [MeV/u]	20	7
Total momentum spread at injection [%]	± 0.12	
Revolution frequency at injection [MHz]	0.810	0.486
Revolution period at injection [μs]	1.23	2.06
Bunch emittance before trapping [eV·s]	0.117	0.827
rf harmonic number *h*	1	
rf stable phase [deg]	0	
$V_{initial}$ [kV]	0.035	0.029
V_{final} [kV]	0.350	0.291
Trapping time [ms]	26.8	40.4
Synchrotron frequency [kHz]	0.806	0.535
Synchrotron period [ms]	1.2	1.9
Bucket acceptance at the end of trapping [eV·s]	0.176	1.323
Filling factor (adiabatic limit = $1/K_{area}$) [%]	66.6	62.5
Total momentum spread after capture [%]	± 0.244	± 0.248
Total energy spread [keV] and [keV/u]	96.0	34.6
Total bunch duration after capture [ns]	818	1267

The analytical calculations provide the input data to run ESME and TSC1D. Figure 3 shows the results. The comparison is possible in the case of the protons, and it can be seen that the space-charge contribution for these energies and intensities does not give any significant increase in the $\Delta p/p$ of the trapped beam. In both cases, the simulations do not show any particle losses.

a)

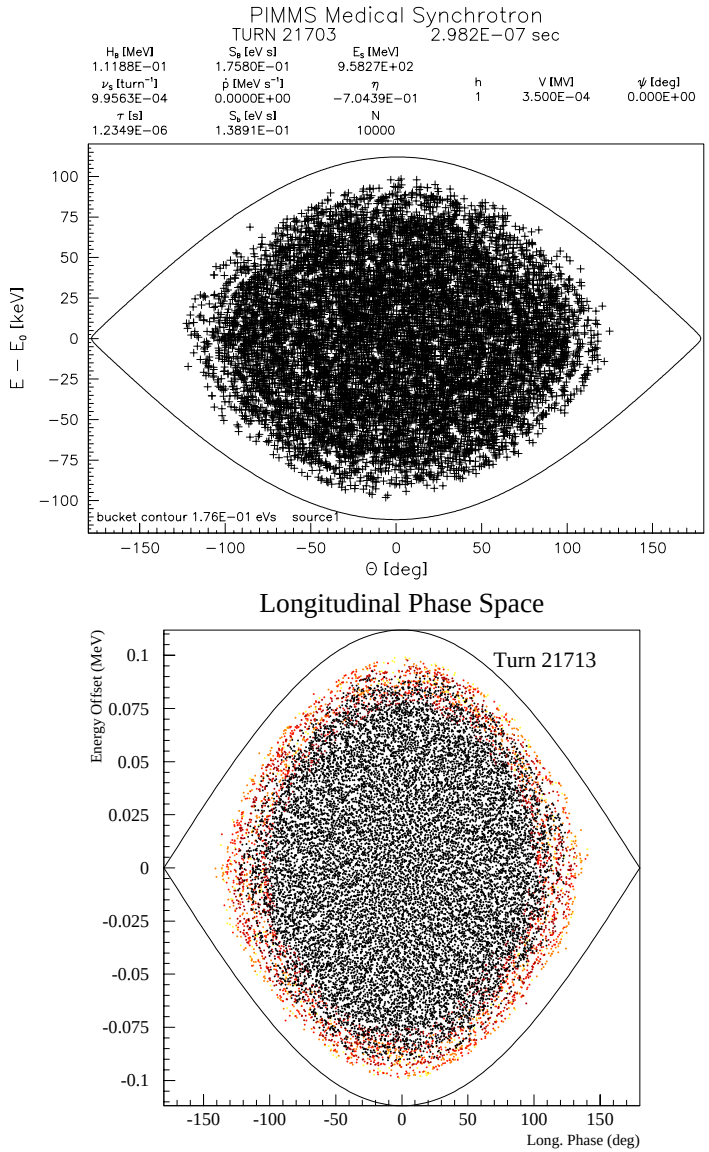

b)

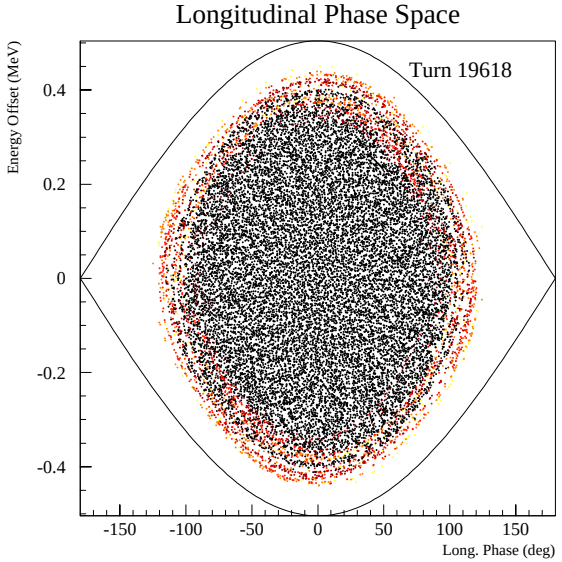

Fig. 3. *Pictures at the end of adiabatic trapping (E-E_0 coincides with the Energy Offset, i.e. the difference between the actual particle energy E and the energy of the synchronous particle E_0):*

a) 20 MeV protons, comparison between ESME (top), no space charge included, and TSC1D (bottom), space charge included.

b) 7 MeV/u carbon (TSC1D).

Note that the Y scale is always in MeV (not MeV/u) for TSC1D plots, whereas it is in keV for ESME plots.

5. THE ACCELERATION

The purpose of the acceleration cycle is to accelerate the beam with as low as possible particle losses and within the hardware limits. The rf system used for particle acceleration is composed of a single gap rf cavity. A description of the hardware and a parameter list are given in [10] and [11]. It is important to limit the maximum values of the rf voltage, of the rf swing, of the rf tuning rate and of the variation of the magnetic field. The losses are minimised by keeping low values for the momentum spread, for the tune shift and having a small ratio between bunch emittance and bucket acceptance, i.e. a low value of the filling factor. Another constraint imposes that the beam transverse dimensions must fit into the acceptance of the machine. The horizontal acceptance in the case of PIMMS, with respect to the central orbit, is -60 mm < x < +35 mm; -60 mm is the inner limit of the magnets good field region [6] and +35 mm is the outer limit given by the electrostatic septum.

The formulae used to calculate the variation of these parameters during acceleration are given in Appendix A. Here, only a description is given of the procedure adopted. All the formulae can be derived establishing the evolution of two variables: the applied rf voltage V and the magnetic field B. The last one is needed to keep the particles in orbit and, during acceleration, it is an increasing function of the time.

The law that links the energy gain to the variation of the magnetic field is given by [9]:

$$q \cdot V \sin \phi_s = 2\pi R \cdot A_n \frac{d(B\rho)}{dt} \qquad (8)$$

where q is the charge of the particle, A_n its mass, R the mean radius of the orbit, and $B\rho$ the magnetic rigidity.

It is common use to establish the magnetic field variation following a cosine-like function. This gives a smooth variation of the field and maintains the value of $\dot{B}(t)$ inside acceptable limits. The rate of acceleration is automatically set by the previous equation.

The question remains how to share this rate between V and $sin\phi_s$. A common procedure to minimise the losses is to keep small bunches inside large buckets. This implies the use of a large voltage, usually the largest allowed by the hardware, and of a correspondingly small phase. On the other hand, at injection energy and during the early stages of acceleration, it is necessary to limit the increase of $\Delta p/p$ and of the tune shifts, which could cause particle losses. The early stages of acceleration are critical because the space-charge effects are stronger and the values of these parameters are larger, as is evident from the formulae of Appendix A. After the adiabatic trapping the value of the voltage is a few hundreds volts. After a certain point in the acceleration, it has been decided to keep the rf voltage constant at the value of about 3 kV. This value is a compromise between the needs of a sufficiently large bucket area and a small $\Delta p/p$.

The time at which the rf voltage reaches this maximum value, as well as the time variation law, is found with an optimisation procedure. The voltage variation has to be a continuous function of time as well as its first derivative, and the adiabatic factor has to be as low as possible.

In Tables 3 and 4 and Figures 4 and 5, the parameters of the rf cycle are presented for the maximum extraction energies. Shown in Appendix B are the cycles for minimum extraction energies. The results are checked with the codes ESME and TSC1D. Both codes showed very similar outputs and no losses.

In Figures 4 and 5, plots (i) and (j), the transverse beam envelope dimensions are also presented. The plots labelled (i) are taken at the point where there are the largest beam dimensions. It is shown that the beam is always kept inside the good field region (inner limit: –60 mm). The plots labelled (j) are taken at the electrostatic septum, and it is shown that during acceleration the beam never hits the septum (position at +35 mm).

Table 3. *20-250 MeV proton acceleration.*

	Injection (after trapping)	Extraction*
Number of protons	6.84×10^{10}	6.84×10^{10}
Kinetic energy [MeV]	20	250
Momentum [GeV/c]	0.195	0.729
Magnetic rigidity [T m]	0.65	2.432
Revolution frequency [MHz]	0.81	2.445
Total momentum spread ($\sqrt{5}$ rms) [%]	± 0.12	≥ ± 0.2
Norm. H&V rms emittance [π mm mrad]	2.5	
Maximum rf voltage [kV]	2.9	
Maximum phase [deg]	16.9	
rf harmonic number h	1	
Frequency swing	3	
Maximum tuning rate [MHz/s]	10.4	
Maximum B(t) field ramp [T/s]	2.6	
Maximum total momentum spread ($\sqrt{5}$ rms) [%]	± 0.331	
Maximum horizontal tune shift	0.08 (at 20.9 MeV)	
Maximum vertical tune shift	0.12 (at 22.6 MeV)	

* After rf gymnastics i.e.: bunch elongation on the unstable fixed point followed by debunching.

Table 4. *7-400 MeV/u $^{12}C^{6+}$ acceleration.*

	Injection (after trapping)	Extraction*
Number of carbon ions	7.9×10^{8}	7.9×10^{8}
Kinetic energy [MeV/u]	7	400
Momentum [GeV/c]	0.114	0.951
Magnetic rigidity [T m]	0.763	6.346
Revolution frequency [MHz]	0.486	2.85
Total momentum spread ($\sqrt{5}$ rms) [%]	± 0.12	≥ ± 0.2
Norm. H&V rms emittance [π mm mrad]	6.1	
Maximum rf voltage [kV]	2.7	
Maximum phase [deg]	20.6	
rf harmonic number h	1	
Frequency swing	5.9	
Maximum tuning rate [MHz/s]	6.0	
Maximum B(t) field ramp [T/s]	2.98	
Maximum total momentum spread ($\sqrt{5}$rms) [%]	± 0.29	
Maximum horizontal tune shift	0.001 (at 7.9 MeV/u)	
Maximum vertical tune shift	0.001 (at 8.3 MeV/u)	

* After rf gymnastics i.e.: bunch elongation on the unstable fixed point followed by debunching.

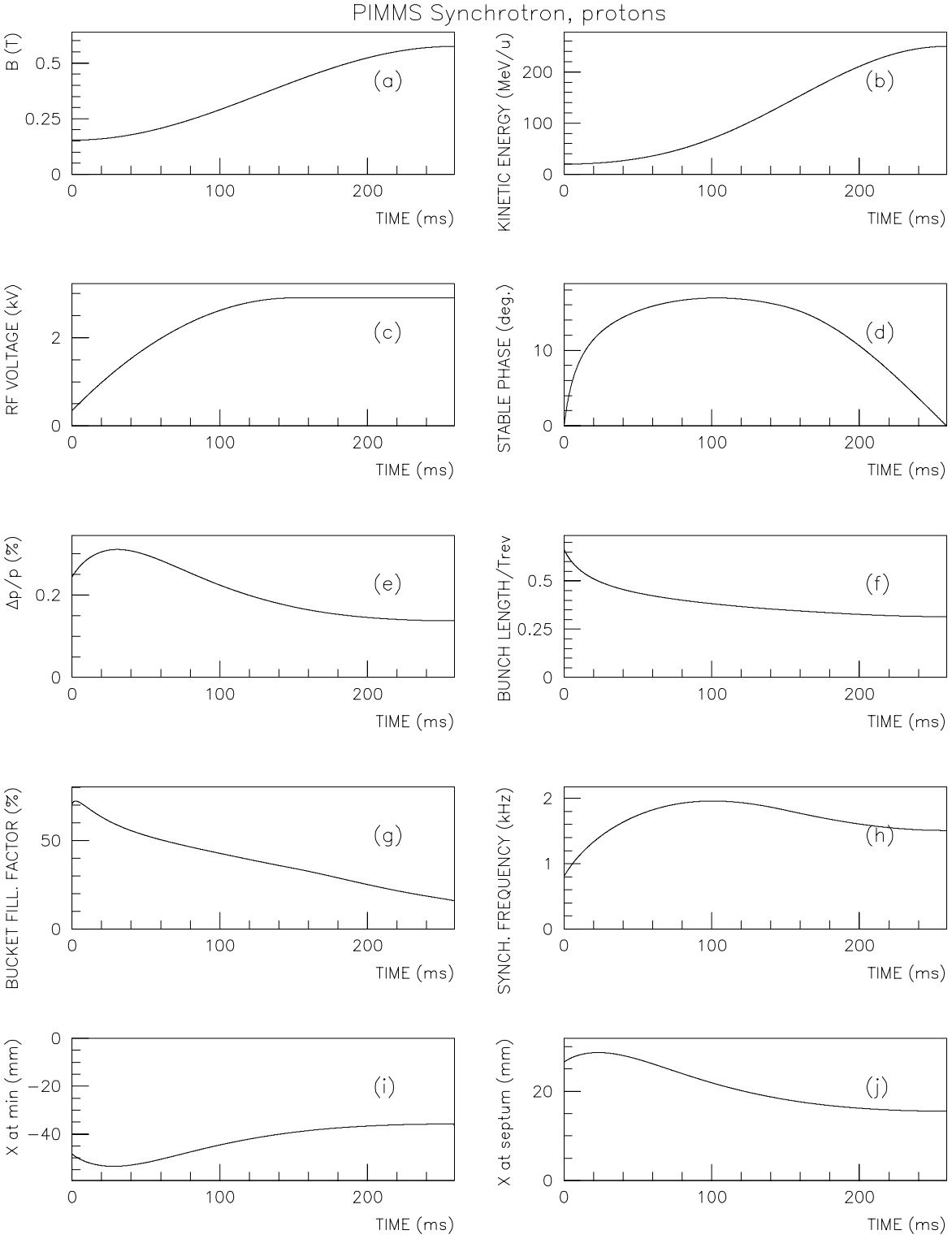

Fig. 4. *20-250 MeV protons: fundamental parameters of the acceleration cycle versus time.*

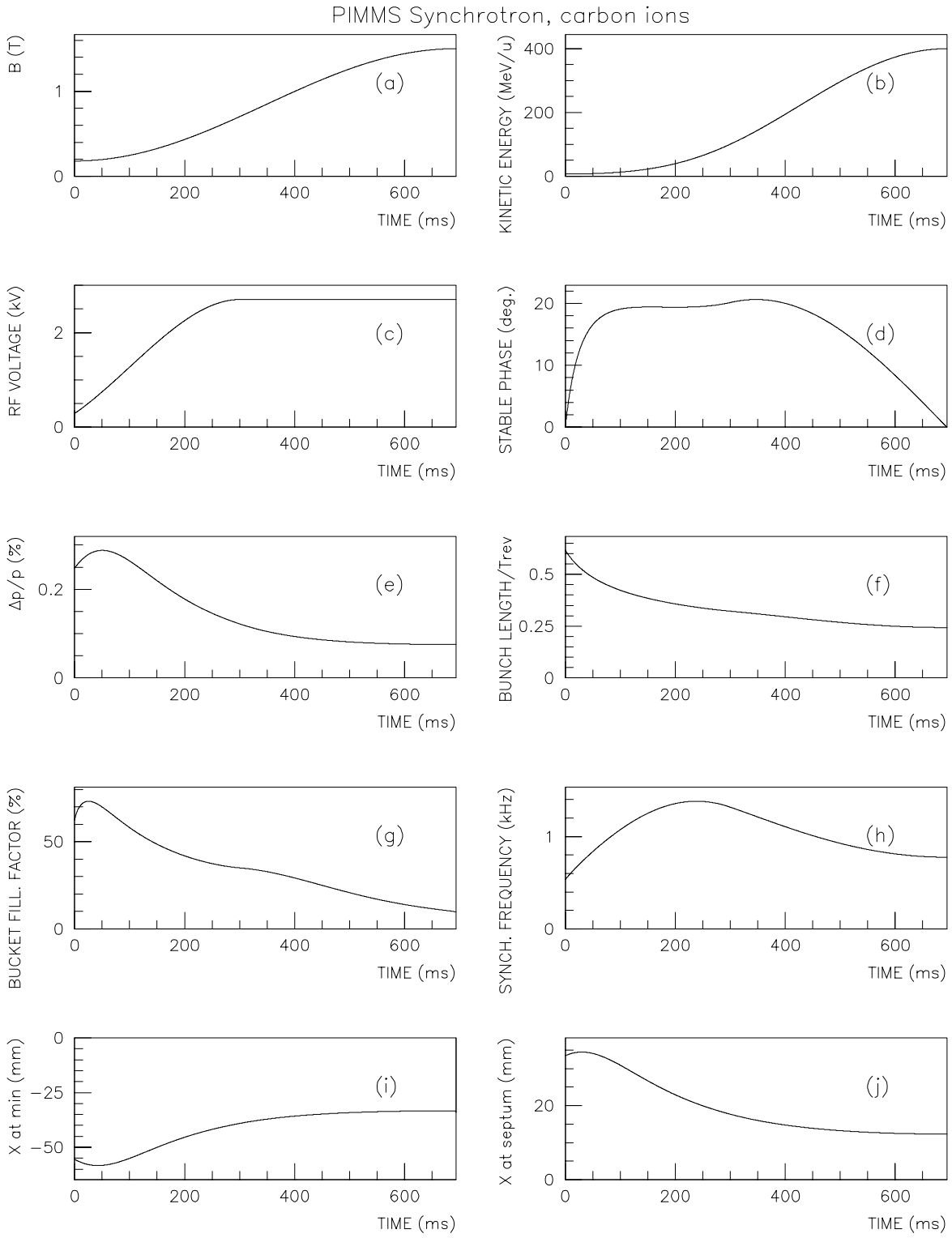

Fig. 5. *7-400 MeV/u $^{12}C^{6+}$: fundamental parameters of the acceleration cycle versus time.*

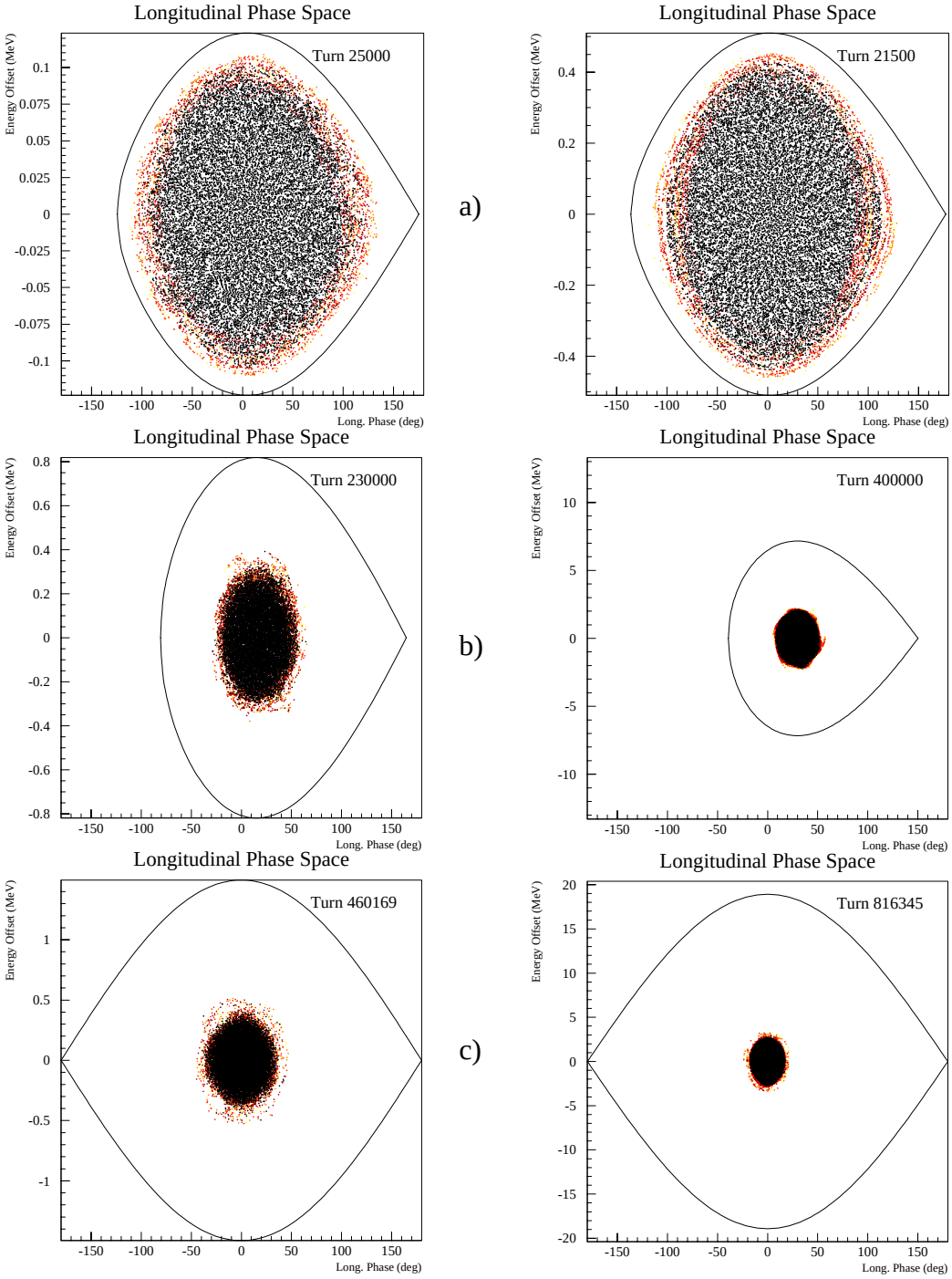

Fig. 6. *Results with TSC1D. Left column protons accelerated from 20 to 250 MeV, right column carbon ions accelerated from 7 to 400 MeV/u. a) First stages of acceleration; b) after 230000 turns for protons and after 400000 turns for carbon; c) end of acceleration. Note that the Y scale is always in MeV (not in MeV/u).*

6. PREPARATION OF THE BEAM FOR EXTRACTION

At the end of the acceleration, in order to obtain the desired beam characteristics for extraction, the bunch needs to be manipulated by the rf system into an unbunched beam with a total $\Delta p/p$ of 0.4 % and with a distribution as uniform as possible. The technique employed should take into account the following constraints:

- the time required for the whole manipulation should not exceed a few tens of milliseconds;
- taking the hardware limitations into account, the rf voltage should not exceed the maximum values established in the acceleration cycle;
- the technique should be as simple as possible.

The process is divided into two steps. See Figures 7a and 7b.

Step one: rf phase jump.
At the extraction energy, after acceleration, the bucket is stationary, i.e. the stable phase equals zero. The rf voltage and frequency maintain the values reached at the end of acceleration, but a phase jump of 180° is performed. The bunch then elongates along the separatrices. The phase remains at this unstable fixed point until the desired $\Delta p/p$ is reached. In the present case, this takes about one hundred microseconds. The procedure is fast, simple to perform from the hardware point of view, and flattens the final distribution.

Step two: debunching.
The rf voltage is abruptly switched off and the beam progressively fills-up the ring, i.e. it debunches. The time needed until the head of the bunch reaches its tail, i.e. the debunching time, is given by [9]:

$$T_{db} = 2 \cdot \frac{\left(\pi - \frac{\Delta \phi_b}{2} \right)}{h \cdot \omega \cdot \eta \cdot \Delta p / p} \qquad (9),$$

where $\Delta\phi_b$ is the bunch length. In the considered cases T_{db} is about 0.15 ms for 250 MeV protons and about 0.2 ms for 60 MeV protons. The time needed to obtain a complete smearing of the particles in the longitudinal phase space (i.e. a nearly uniform distribution of particles around the ring) is longer. It has been decided to reserve a maximum of 30 ms for the whole process.

The rf phase jump is very rapid, so that the analytic program RFAC used to simulate the acceleration cannot be used. Indeed, the condition for the process to be adiabatic is not fulfilled. In this case ESME is used to simulate the process. The analysis is therefore limited to protons. The simulations for 60 and 250 MeV extraction energies are presented in Figures 7a and 7b respectively.

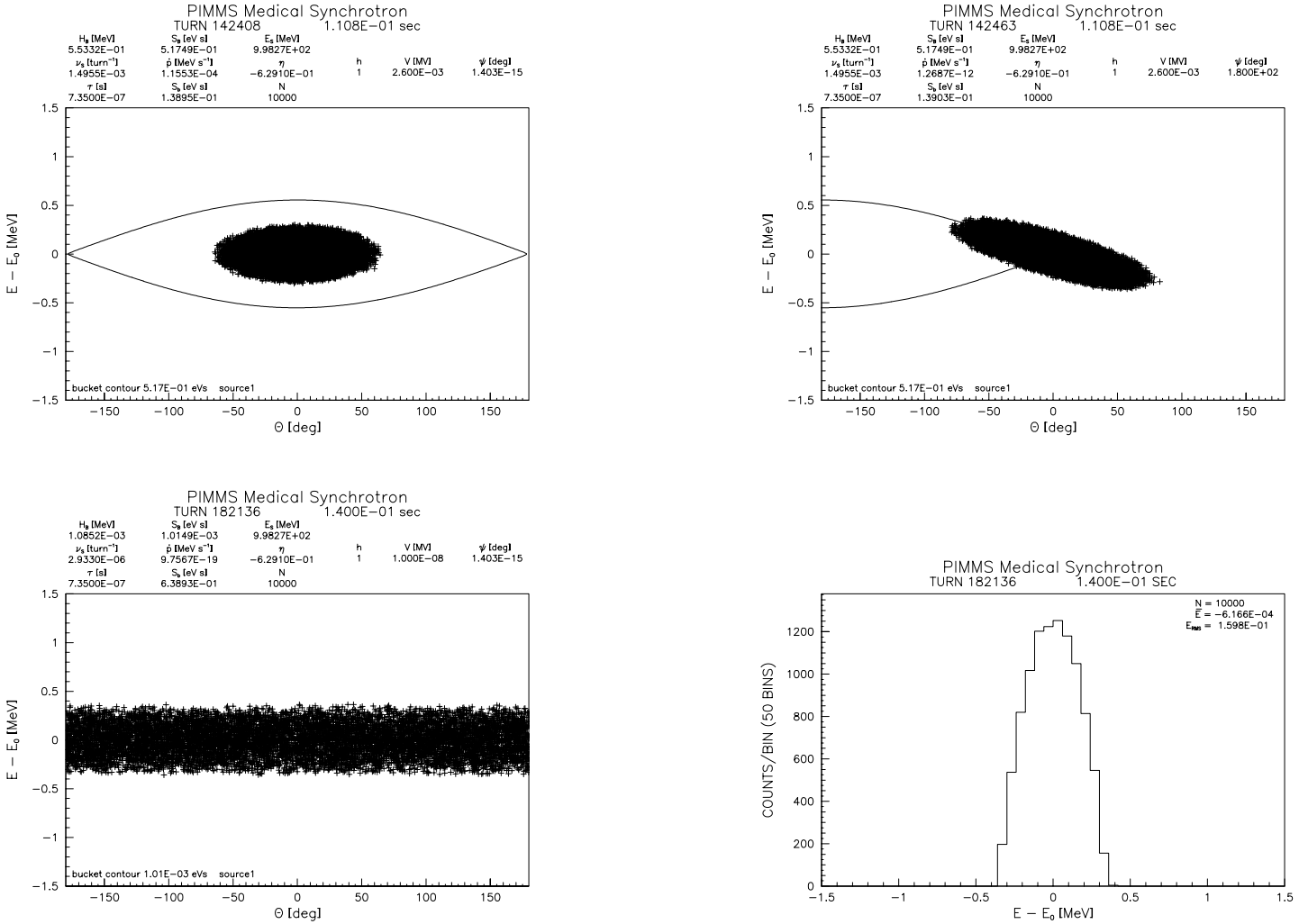

Fig.7a. *Example of ESME simulation for 60 MeV protons: top left) end of acceleration; top right) end of phase jump; bottom left) 30 msec after rf switch off; bottom right) final beam distribution in ΔE.*

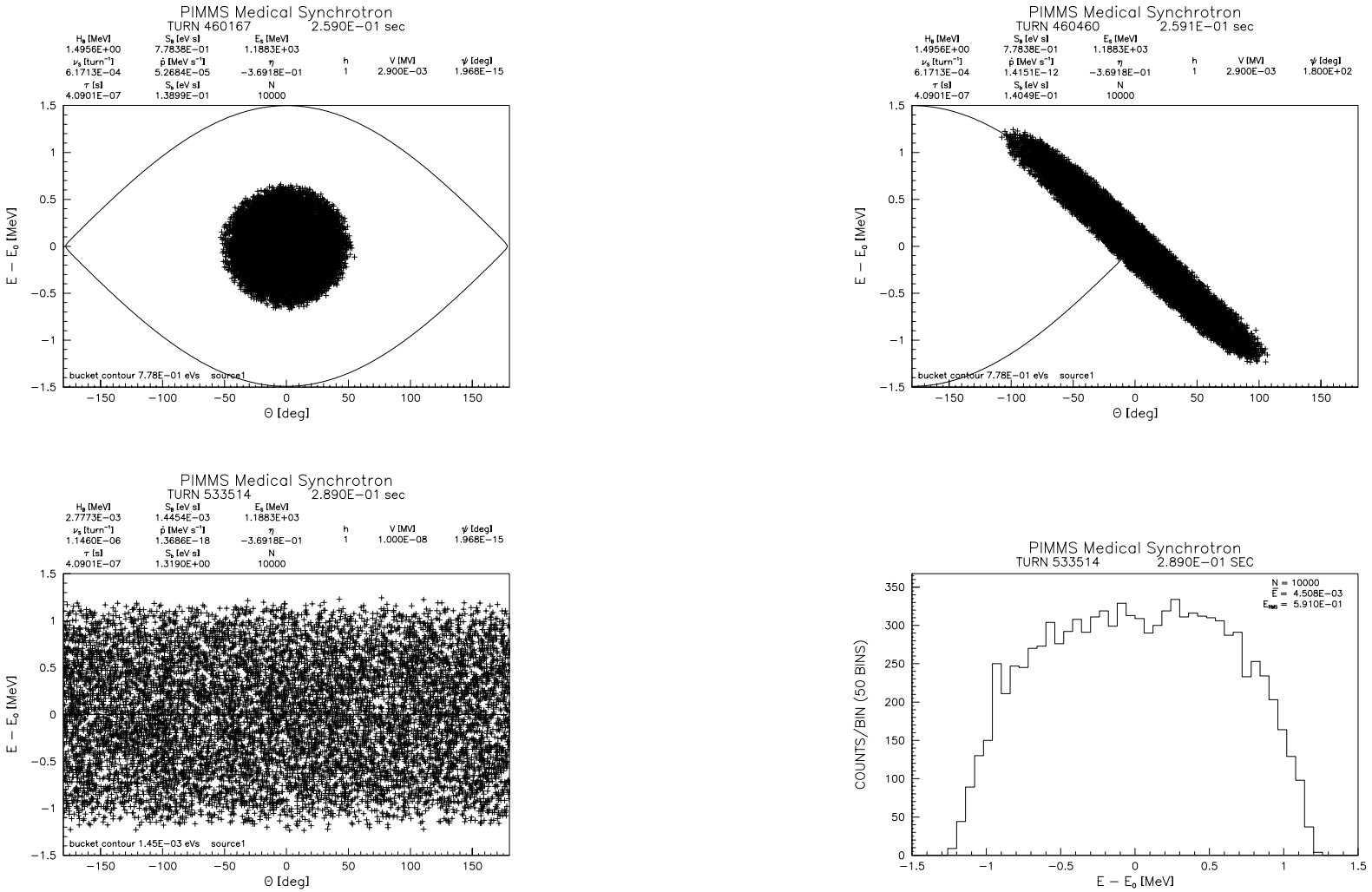

Fig. 7b. *Example of ESME simulation for 250 MeV protons: top left) end of acceleration; top right) end of phase jump; bottom left) 30 msec after rf switch off; bottom right) final beam distribution in ΔE.*

7. CONCLUSION

The study has shown the feasibility of the rf cycle for protons and carbon ions within the requirements of the PIMMS synchrotron. The results take into account space-charge effects that have some effect for protons at injection and in the early phases of acceleration. The values of the parameters of the cycles are set according to the available hardware parameters, i.e. the rf cavity and the magnet cycle, and to satisfy the constraints imposed by the beam dynamics in the transverse phase planes.

8. ACKNOWLEDGEMENTS

The authors have benefited from fruitful discussions with P. Bryant (PIMMS Project Leader), W. Pirkl (CERN), M. Pullia and M. Weiss (TERA). The help and support of S. Hancock (CERN) and C. Prior (RAL) was much appreciated. The authors also wish to thank the PS Division of CERN for hosting this study.

REFERENCES

[1] J. MacLachlan, *User's Guide to ESME v. 8.2*, Fermilab, Chicago (1996).

[2] P. Knaus, *Simulation of Space Charge Dominated Beams and Experimental Tests*, Ph.D. thesis, Inst. f. Exp. Kernphysik, Univ. Karlsruhe (TH), to be published.

[3] P. Bryant, Private Communication, *Space-Charge Tune Shifts at Injection*, Informal Meeting No. 4 on Slow Extraction from Synchrotrons for Cancer Therapy, CERN (September 1997).

[4] C.R. Prior, *Computer Simulation of the Motion of Charged-Particle Beams under Space-Charge*, Rutherford Appleton Laboratory, U.K., RAL-TR-1998-048.

[5] A. Hofmann, *Single Beam Collective Phenomena – Longitudinal*, Proc. of the First Course of the International School of Particle Accelerators of the Ettore Majorana Centre for Scientific Culture, Erice, Italy, (1976), CERN 77-13 (1977) p.139-174.

[6] P. Bryant, M. Pullia, Private Communication, *Final Choice of the Synchrotron Magnet Cycle*, (March 1999).

[7] U. Bigliani, *Système HF du Booster. Capture dans l'espace de phase longitudinal*, CERN/SI/Int. EL/68-2 (1968).

[8] D. Boussard, *RF techniques for pp-bar*, Proc. of the CERN Accelerator School – Antiprotons for colliding beam facilities, Geneva (October 1983), CERN 84-15 (1984) Vol. I, p.261-290.

[9] C. Bovet, R. Gouiran, I. Gumowski, K.H. Reich, *A Selection of Formulae and Data Useful for the Design of A.G. Synchrotrons*, CERN/MPS-SI/Int. DL/70/4 (1970).

[10] M. Crescenti, G. Primadei, A. Susini, *A New Compact Large Frequency-Swing RF System for Hadron Acceleration: Test Results*, CERN/PS 97-60 (DI) (1997).

[11] Fondazione TERA, *Il Centro Nazionale di Adroterapia Oncologica a Mirasole*, ed. INFN-LNF Frascati, Roma (Febbraio 1997), Capitolo 6, p.87-120.

[12] G. Dôme, *Theory of RF Acceleration*, CERN 87-03 (1987), p.110-158.

[13] W. Pirkl, *Longitudinal beam dynamics*, CERN 95-06 (1995), p.233-257.

[14] B. Gottschalk, *Design of a Hospital-Based Accelerator for Proton Radiation Therapy: Scaling Rules*, Nucl. Instr. and Meth. B24/25 (1987), p.1092-1095.

[15] P. Knaus, *Signal Denoising Using Wavelets*, CERN/SL (1999), to be published.

[16] I. Daubechies, *Ten Lectures on Wavelets*, SIAM Lecture Series in Applied Mathematics, Vol. 61, SIAM, Philadephia (1992).

[17] Ch. J. Isham, *Lectures on Groups and Vector Spaces for Physicists*, World Scientific Lecture Notes in Physics, Vol. 31, World Scientific, Singapore (1989).

[18] A. Louis, P. Maass, A. Rieder, *Wavelets: Theorie und Anwendungen*, Teubner, Stuttgart (1994).

[19] Ponenti, *Numerical Algorithms based on biorthogonal Wavelets*, IRPHE, Marseille, (1995).

[20] Jameson, *On the Wavelet Optimized Finite Difference Method*, Inst. for Comp. Appl. in Sci. and Eng., Hampton, U.K. (1994).

APPENDIX A: BASIC EXPRESSIONS

For a detailed analysis of the longitudinal beam dynamics the reader is referred to Refs [12] and [13]. It is useful to recall here, a few important expressions that are used in the text.

The motion in the longitudinal phase plane, neglecting space-charge effects, can be described in terms of two first order differential equations in the canonically conjugated variables $\Delta E/h\omega_s$, *and* $\Delta\phi$:

$$\frac{d}{dt}\left(\frac{\Delta E}{h\omega_s}\right) = \frac{q(V(\phi) - V(\phi_s))}{2\pi h} \qquad \Delta E = E - E_s$$

$$\frac{d(\Delta\phi)}{dt} = -\omega_s^2 h^2 \frac{\eta}{\beta^2 E}\left(\frac{\Delta E}{h\omega_s}\right) \qquad \Delta\phi = \phi - \phi_s$$

where q is the charge, ω_s is the revolution frequency, $V(\phi) = V\sin\phi$ is the rf voltage, $\beta = v/c$ is the particle normalised velocity, h is the harmonic number, $\eta = 1/\gamma^2 - 1/\gamma_\tau^2$ is the phase slip factor, γ is the relativistic factor, γ_t the relativistic factor at transition, E is the total (kinetic + rest) energy, ϕ is the phase of the arbitrary particle and corresponds to the phase of the rf voltage, and "*s*" refers to the synchronous particle.

The choice of two canonically conjugated variables is justified by the opportunity to describe the motion using the Hamiltonian, which represents the total energy of the particle and, in the hypothesis of a conservative system, is a constant of the motion.

$$H = \frac{1}{2}\frac{\eta}{\beta^2 E}(\Delta E)^2 + \frac{qV}{2\pi h}U(\phi)$$

where:

$$U(\phi) = \sin\phi_s(\phi_s - \phi) + \cos\phi_s - \cos\phi$$

In the adiabatic limit, i.e. when the longitudinal dynamic is slow enough for the bunch to stay matched, the bunch behaviour is described by the Hamiltonian of the limiting particle trajectory inside the bucket.

Under these hypotheses, a list of the main useful formulae are presented:

a) Formulae for the bucket:

The bucket half height:

$$\Delta E = \sqrt{\frac{\beta^2}{\eta}\frac{qVE}{\pi h}}\,Y(\phi_s)$$

The bucket momentum acceptance (it corresponds to the maximum value of the momentum spread along the separatrix):

$$\left(\frac{\Delta p}{p}\right)_B = \frac{2}{\beta}\sqrt{\frac{qV}{\eta\pi hE}}\cdot Y(\phi_s)$$

with: $Y(\phi_s) = \sqrt{\sin\phi_s(2\phi_s - \pi) + 2\cos\phi_s}$ being a decreasing function of ϕ_s [12].

The bucket width:

$$\Delta\phi_B = \phi_u - \phi_l$$

with $\phi_u = \pi - \phi_s$ (direct evaluation)
$U(\phi_l) = U(\phi_u) \Rightarrow \phi_l$ (implicit evaluation)

b) Formulae for the bunch:

The bunch momentum spread:

$$\left(\frac{\Delta p}{p}\right)_b = 2\frac{\sqrt{A_b}}{\beta}\left(\frac{2hc^2 qV\cos\phi_s}{\pi C^2\eta E^3}\right)^{1/4}$$

The bunch length:

$$\Delta t_b = 2\frac{\sqrt{A_b}}{\beta}\left(\frac{C^2\eta}{2\pi^3 hc^2 qEV\cos\phi_s}\right)^{1/4}$$

where C is the machine circumference and A_b the bunch area.

The tune shifts. They are due to the defocusing action of the space charge that produces an incoherent tune shift [14] given by:

$$\Delta Q_{x,y} = -\frac{Z^2}{A_n}\frac{r_0}{2\pi}\frac{1}{\beta\gamma^2}\frac{N_p}{\varepsilon^*_{x,y}}\frac{1}{B_f}$$

where Z is the atomic number, A_n the mass number, r_0 the classical proton radius, N_p the number of particles, $\varepsilon^*_{x,y}$ the total normalised transverse emittances in π *mm mrad*.
B_f is the bunching factor defined as the ratio between the average and the peak beam currents, i.e.:

$$B_f = \frac{I_{average}}{I_{peak}} \div \frac{\Delta t_b}{T_{revolution}}$$

It is easy to derive:

$$\Delta Q_{x,y} \div \left(\frac{V \cos \phi_s}{E^7} \right)^{1/4}$$

c) Formulae for the synchrotron:

The basic formula that gives the energy gain is:

$$q \cdot V \sin \phi_s = 2\pi R \cdot A_n \frac{d(B\rho)}{dt}$$

The momentum variation:

$$\frac{dp}{dt} \div \frac{q}{A_n} \frac{d(B\rho)}{dt}$$

The rf frequency:

$$f = \frac{h\beta c}{C}$$

APPENDIX B: CYCLES AT MINIMUM EXTRACTION ENERGY

Table B1. 20-60 MeV protons acceleration.

	Injection (after trapping)	Extraction*
Number of protons	6.84×10^{10}	6.84×10^{10}
Kinetic energy [MeV]	20	60
Momentum [GeV/c]	0.195	0.340
Magnetic rigidity [T m]	0.65	1.137
Revolution frequency [MHz]	0.81	1.361
Total momentum spread ($\sqrt{5}$ rms) [%]	± 0.12	≥ ± 0.2
Norm. H&V rms emittance [π mm mrad]	2.5	
Maximum rf voltage [kV]	2.6	
Maximum phase [deg]	11.5	
rf harmonic number h	1	
Frequency swing	1.7	
Maximum tuning rate [MHz/sec]	7.8	
Maximum B(t) field ramp [T/s]	1.63	
Maximum total momentum spread ($\sqrt{5}$ rms) [%]	± 0.351	
Maximum horizontal tune shift	0.08 (at 20.8 MeV)	
Maximum vertical tune shift	0.12 (at 23.2 MeV)	

* After rf gymnastics i.e.: bunch elongation on the unstable fixed point followed by debunching.

Table B2. *7-120 MeV/u $^{12}C^{6+}$ acceleration.*

	Injection (after trapping)	Extraction*
Number of carbon ions	7.9×10^{8}	7.9×10^{8}
Kinetic energy [MeV/u]	7	120
Momentum [GeV/c]	0.114	0.488
Magnetic rigidity [T m]	0.763	3.254
Revolution frequency [MHz]	0.486	1.85
Total momentum spread ($\sqrt{5}$ rms) [%]	± 0.12	≥ ± 0.2
Norm. H&V rms emittance [π mm mrad]	6.1	
Maximum rf voltage [kV]	2.5	
Maximum phase [deg]	21.6	
rf harmonic number h	1	
Frequency swing	3.8	
Maximum tuning rate [MHz/sec]	6.45	
Maximum B(t) field ramp [T/s]	2.72	
Maximum total momentum spread ($\sqrt{5}$ rms) [%]	± 0.297	
Maximum horizontal tune shift	0.001 (at 7.9 MeV/u)	
Maximum vertical tune shift	0.002 (at 8.4 MeV/u)	

* After rf gymnastics i.e.: bunch elongation on the unstable fixed point followed by debunching.

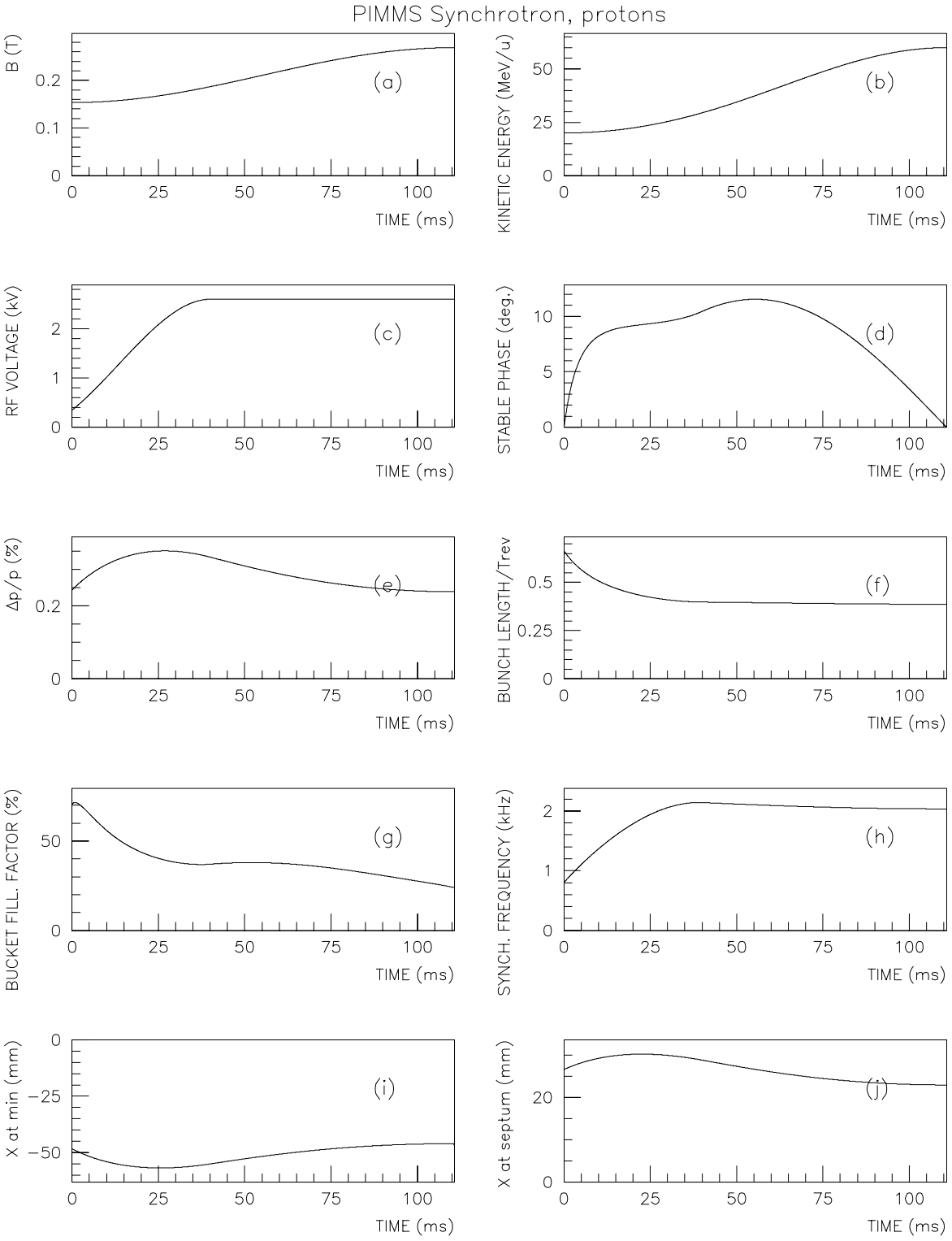

Fig. B1. *20-60 MeV protons: fundamental parameters of the acceleration cycle versus time.*

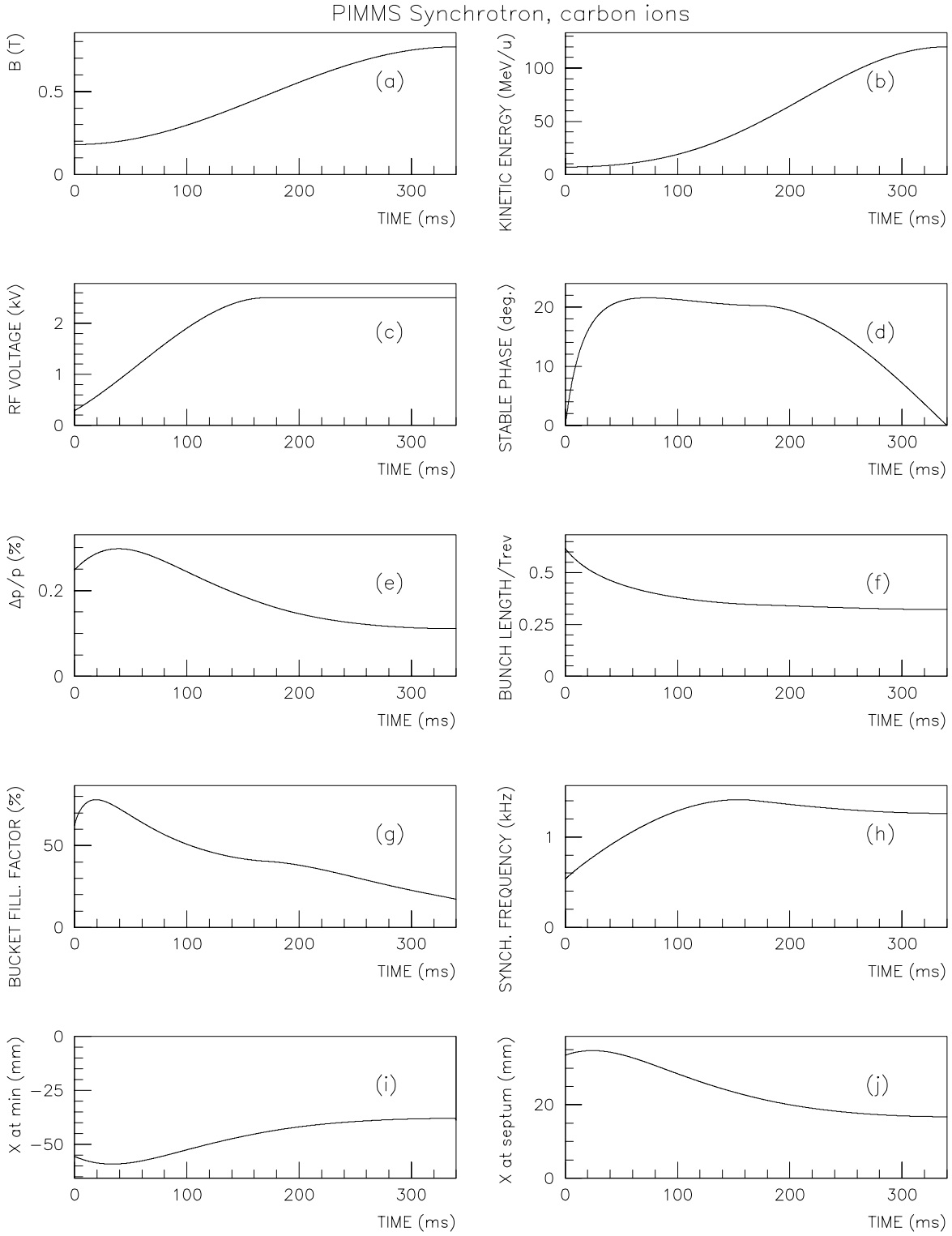

Fig. B2. *7-120 MeV/u $^{12}C^{6+}$: fundamental parameters of the acceleration cycle versus time.*

APPENDIX C: INTRODUCTION TO TSC1D

Solution of Poisson's Equation Using Wavelets.

The basic problem encountered by a particle tracking code that takes direct space-charge effects into account is the fast and precise solution of the underlying partial differential equation: the Poisson equation. This holds particularly for time intensive two-dimensional transverse and even more so for three-dimensional simulations. The one-dimensional Poisson solver of the longitudinal code TSC1D was developed as a test bench for a wavelet-based tracking code in order to gain experience with this new numerical method. In this section the basic framework required to understand the usefulness of wavelets for the solution of Poisson's equation is outlined.

The Mathematical Framework: Multiresolution Analysis (MRA)

An intuitive understanding of the MRA may be provided by comparing it to the approximation of a fraction of integers by decimals, e.g. $193/17 \approx 11.35294...$ The scaling function, compressed or dilated, gives an image of the signal at a given resolution, just as one can round off 193/17 to 10, 11, 11.3 or 11.35... depending on the desired accuracy. Wavelets encode the difference of information between two resolutions differing by a factor of two, whereas the different levels of resolution for decimals differ by a factor of 10. Between the approximate values 10 and 11 of the initial fraction, wavelets encode the detail 1, between 11 and 11.3 other, smaller wavelets encode the details 0.3, between 11.3 and 11.35 still others encode 0.05, and so forth.

The more one goes down in the level of resolution, the better the approximation. In the other direction, stretching the scaling function more and more, one ends by seeing nothing at all, as if one was trying to approximate 193/17 by hundreds and thousands. At that point all the information has been treated like details encoded by the wavelets 10+1+0.3+0.05+0.002+.... .This feature of coarsening the resolution may indeed be used for signal denoising or data smoothing [15].

In a very analogous manner the mathematical framework of a MRA [16], [17] is based on two fundamental concepts: nested subspaces and orthonormal bases allowing decomposition of information into different scales. On top of these, there is a third ingredient, the invariant of the basis functions under certain translations (in each subspace) and dilation (from one subspace to another). Thus, all the basis functions are nothing else than scaled and translated versions of one shape function, the scaling function.

Thus, the MRA provides a framework that systematically separates details and coarse scale properties. What makes the MRA special is the fast and stable way in which it does the job.

The wavelet-based numerical algorithm

The main advantage of wavelet methods for the solution of Poisson's equation lies in their ability to zoom into regions of steep gradients or cuts in the beam distribution as occurring for example in case of a multi-turn injection with transverse beam loss on the septum plate. However, in the case of longitudinal dynamics, the one-dimensional charge

distribution is generally smooth on a large scale (if micro-bunching from the injector is neglected) and consequently only few different scales of resolution need to be considered.

Two alternative approaches exist to exploit wavelets and the MRA framework for a more efficient solution of partial differential equations. A very elegant but mathematically demanding method consists in using wavelets directly as a set of basis functions in an adaptive wavelet-Galerkin method [18]. First a suitable basis set needs to be found knowing that numerical efficiency of the algorithm basically imposes biorthogonal wavelets [19]. In order to satisfy the periodic boundary conditions of the charge distribution in longitudinal phase space, the coefficients of the corresponding boundary adapted wavelets need to be determined. The charge distribution is then developed in this basis and the thus obtained series coefficients serve as an initial guess of the solution. Application of the Laplace operator in its wavelet representation then leads to a preconditioned sparse system of linear equations that may be solved rapidly by standard methods. The complete algorithm and underlying mathematics are described in detail in [2].

In the second approach the magnitude of the wavelet series is not used to decide which basis functions to use in a Galerkin approach, but to decide which grid points of an equidistant computational mesh are worthwhile considering, and which ones may de rejected. This leads to a refined mesh with a minimum number of mesh points as can be seen in Figure C1.

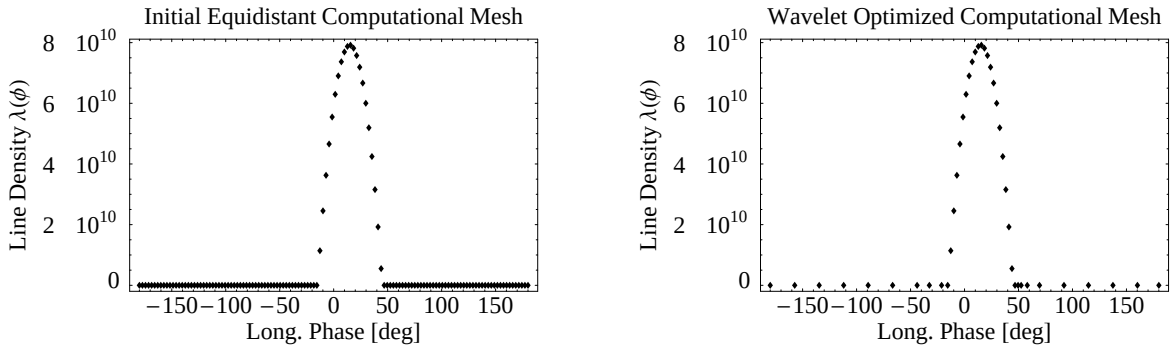

Figure C1. *The left hand figure shows the initial 128 equidistant points of the computational mesh on which the line density of a parabolic bunch is discretised. This situation represents the ideal bunch shape after about 230.000 machine revolutions for the proton rf cycle. Instead, the right-hand plot represents the wavelet optimized dyadic grid making use of eight levels of resolution and consisting of 46 points only. This reflects directly the gain in computer time by a factor of three, however reduced by the effort put in the mesh refinement.*

Poisson's equation is thus solved on the refined dyadic grid using either finite differences [20] or finite elements. Generalization to two dimensions is straightforward by simply applying the one-dimensional refinement first to all columns, then to all rows of the two-dimensional mesh. The full power of both methods becomes obvious once steep gradients occur in the charge distribution, e.g. when studying longitudinal micro-bunch dynamics or transverse multi-turn injection with septum losses.